Chinese Chemical Letters 32 (2021) 3226–3230

Contents lists available at ScienceDirect

Chinese Chemical Letters

journal homepage: www.elsevier.com/locate/cclet

Communication

0D/1D AgI/MoO_3 Z-scheme heterojunction photocatalyst: Highly efficient visible-light-driven photocatalyst for sulfamethoxazole degradation

Jing Xu[1], Juan Chen[1], Yanhui Ao*, Peifang Wang

Key Laboratory of Integrated Regulation and Resource Development on Shallow Lakes of Ministry of Education, College of Environment, Hohai University, Nanjing 210098, China

ARTICLE INFO

Article history:
Received 16 December 2020
Received in revised form 14 February 2021
Accepted 5 March 2021
Available online 3 April 2021

Keywords:
MoO_3-based-photocatalyst
0D/1D
Z-scheme
Sulfamethoxazole
Visible-light-responsive

ABSTRACT

Low dimension nano photocatalysts show great potential in the field of treating contaminated water for their large surface area and size effect. In this study, a 0D/1D AgI/MoO_3 Z-scheme photocatalyst with striking photocatalytic performance was constructed successfully. The one-dimensional MoO_3 nanobelts were prepared by a simple hydrothermal method, and then it was modified by AgI nanoparticles in a handy deposition approach. When choosing sulfamethoxazole (SMZ) as the target contaminant, the rate constant value of the optimal 0D/1D AgI/MoO_3 composite could hit up to 0.13 min^{-1}, which is nearly 22.4 times and 32.5 times as that of pure MoO_3 (0.0058 min^{-1}) and AgI (0.0040 min^{-1}), respectively. A series of detailed characterizations give evidences that the charge transfer in the composite followed Z scheme mechanism. Therefore, efficient separation/transfer and the remained high redox activity of photo-generated carriers played a vital role in the sharply enhanced photocatalytic properties. The possible degradation pathways of SMZ were proposed based on the intermediates detected by high-performance liquid chromatography-mass spectrometry (HPLC-MS). Meanwhile, the magnificent cyclic stability makes the material a promising material in the practical application.

Pharmaceuticals and personal care products (PPCPs) recently have been frequently detected in various water environmental matrices, for lots of them are under heavy use and difficult to be naturally degraded [1,2]. What is worse, some of them, especially antibiotics, have already brought threat to human health and environmental safety even at a very low level [3–5]. However, traditional water treatment technologies have limitations in treating these emerging contaminants. Thus, finding proper methods to decompose and mineralize them is of great urgency. In all kinds of strategies, advanced oxidation processes have been proved versatile methods in treating contaminated water [6,7]. Among them, photocatalysis has been proven as a rather promising approach for its attractive solar energy conversion ability, outstanding redox ability, low cost, low toxicity, and talent to function under diversified ambient conditions [8–11]. To develop photocatalysts of high degradation and mineralization efficiency, various semiconductor catalytic materials have been studied. MoO_3, as an intrinsic n-type semiconductor with high thermal and chemical stability, has attracted particular interest recently due to its optical properties, nontoxicity, and extensive sources [12–15]. As a transition-metal oxide, MoO_3 has a high positive potential of the valence band, which makes MoO_3 an attractive photocatalyst for the oxidation of pollutants. Moreover, based on the previous study, the shape and size of MoO_3 prepared according to different synthetic strategies has significantly influence on its catalytic performance, among which, a one-dimensional nanostructured MoO_3 has drawn attention due to its large surface area and abundant active sites for catalytic degradation [16,17]. However, MoO_3 has some shortcomings, such as limited electrical conductivity, high recombination rate of charge carriers and low reduction capacity, which bring restriction to its practical application [18].

Recent studies have shown great success in improving catalytic performance of single materials by constructing heterojunctions which not only increase light harvesting capacity but speed up charge separation and transfer [19–23]. Among them, the Z-scheme system has become hotspot in the field of photocatalysis for improving redox capacity to a great extent [24,25]. As it can keep the high reducing capacity from the reduction semiconductor with high conduction band (CB) position and the high oxidation

* Corresponding author.
E-mail address: andyao@hhu.edu.cn (Y. Ao).
[1] These authors contribute equally to the work.

https://doi.org/10.1016/j.cclet.2021.04.003

capacity from the oxidation semiconductor with low valence band (VB) position [26–28]. Hence, choosing semiconductors with proper CB and VB edge positions to construct a Z-scheme system heterojunction is an excellent way to optimize the photocatalytic performance of semiconducting materials. Among all these semiconductors, AgI is an anticipated candidate for its good light sensitivity, benign photocatalytic performance, and suitable band position [29–31]. Recent studies have shown some successes in maximizing photocatalysts activity by building AgI-based direct Z-scheme heterojunction [32–34]. Thus, we believe that it is a worthwhile attempt to construct a Z-scheme system by combining AgI nanoparticles with MoO_3 nanobelts.

Against this background, a 0D/1D AgI/MoO_3 Z-scheme heterojunction photocatalyst was obtained, aiming to achieve materials with high activity for antibiotics degradation under visible light irradiation. SMZ was chosen as the main target contaminant to reveal the degradation performance and operational principle of 0D/1D AgI/MoO_3 composite materials in detail. In addition, a series of tests were conducted to systematically investigate the morphology, structure, optical properties and photoelectrochemical properties of the as-prepared materials to provide a reference for the investigation of mechanism and practical application of 0D/1D AgI/MoO_3 Z-scheme photocatalysts.

The Fig. 1a depicts the synthesis process of 0D/1D AgI/MoO_3 composites, the details can be found in Supporting information. The morphology and microstructure of the as-prepared samples were investigated by scanning electron microscopy (SEM) and transmission electron microscope (TEM) characterizations. It could be observed that MoO_3 shows obvious nanobelts morphology with an average width of about 180 nm and length of more than 3 μm (Figs. 1b and e). For pure AgI, uneven large particles clustering together were observed with an average size of more than 500 nm (Fig. 1c). However, in Fig. 1d, much smaller AgI particles closely anchor and adhere to the surface of MoO_3 nanobelts. This phenomenon validates that the growth and agglomeration of these AgI particles are suppressed in the formation process of the AgI/MoO_3 nanocomposites because of the interaction between the AgI and the MoO_3 surface, which is beneficial to charge transfer. The intimate interfaces between the MoO_3 and AgI can also imply that AgI/MoO_3 nanocomposites are heterojunction in structure rather than a physical mixture of two separate phases (Fig. 1f). The high-resolution transmission electron microscope (HRTEM) gives information about the lattice fringe of the materials. In the HRTEM image of AM-50 (Fig. 1g), the measured d-spacing of 0.33 nm and 0.20 nm corresponded to the (040) and (112) lattice planes of MoO_3 and AgI, respectively, which confirms the AgI particles modified MoO_3 nanobelts heterojunction materials are successfully constructed.

The crystal structures and phase purities of the as-prepared composites were determined by X-ray diffraction (XRD) analysis. As shown in Fig. 2a, the characteristic diffraction peaks of MoO_3 are at 12.8°, 23.4°, 25.7°, 27.3°, 29.7°, 39.0° and 58.8°, relating to the (020), (110), (040), (021), (130), (060) and (081) planes, respectively. It is in good agreement with the standard peaks for the orthorhombic phase of MoO_3 crystallites (JCPDS No. 05-0508). The pure AgI shows the diffraction peaks at 22.3°, 23.7°, 25.4°, 39.2°, 42.6° and 46.3°, which could be ascribed to (100), (002), (101), (110), (103) and (112) crystal planes of the hexagonal phase AgI (JCPDS No. 09-0374). Also, the AM-50 heterostructure obviously exhibits two groups of diffraction peaks that correspond to AgI and MoO_3, respectively. Moreover, as the mass ratio of AgI increases, the peak intensity corresponding to (100), (002) and (112) lattice plane of AgI becomes stronger, indicating the 0D/1D AgI/MoO_3 composite materials are well synthesized (Fig. 2b). Also, it is obvious that no characteristic peaks of other impurities appear and the diffraction peak positions in the XRD patterns hardly change, indicating that the synthesized samples are pure with little structure change.

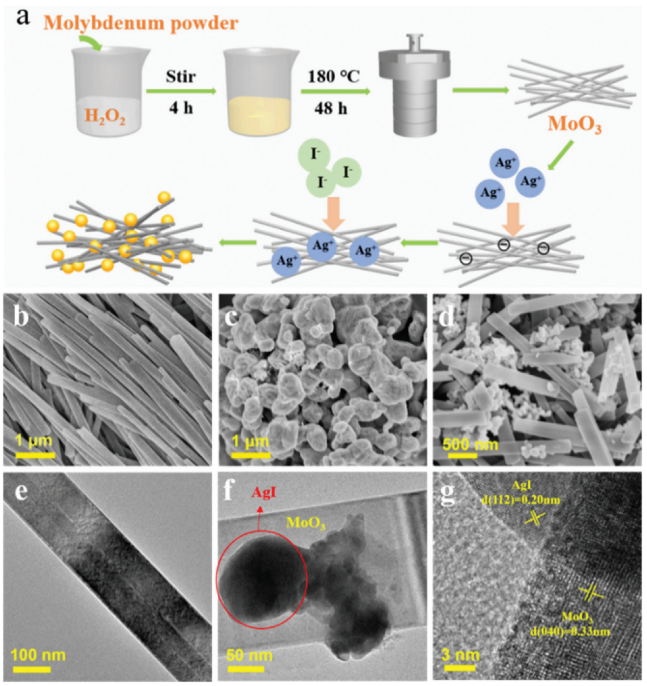

Fig. 1. Synthesis process of 0D/1D AgI/MoO_3 nanocomposites (a). SEM images of MoO_3 (b), AgI (c), AM-50 (d). TEM images of MoO_3 (e), AM-50 (f). HRTEM images of AM-50 (g).

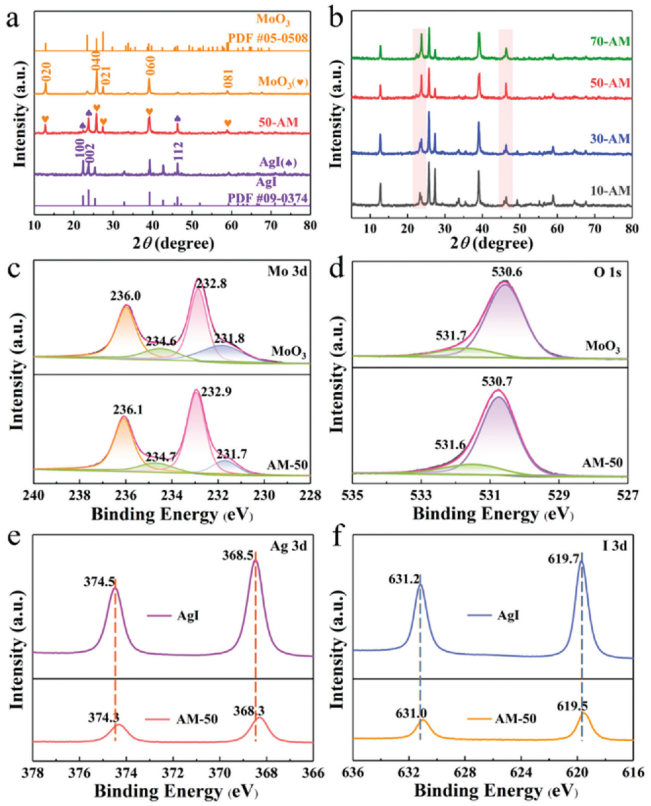

Fig. 2. XRD patterns of as-prepared samples (a, b). High-resolution XPS spectra of MoO_3 and AM-50: Mo 3d (c), O 1s (d). High-resolution XPS spectra of AgI and AM-50: Ag 3d (e), I 3d (f).

The surface compositions and chemical states of MoO_3, AgI and AM-50 were further investigated by X-ray photoelectron spectroscopy (XPS). For Mo 3d, four bands can be observed, which correspond to two different oxidative states. The two peaks at 236.0 eV (Mo $3d_{3/2}$) and 232.8 eV (Mo $3d_{5/2}$) indicate the presence of Mo^{6+} (Fig. 2c) [35]. While, the weaker spectra peaks at 234.6 eV (Mo $3d_{3/2}$) and 231.7 eV (Mo $3d_{5/2}$) are attributed to the existence of Mo^{5+} [36], demonstrating the minor existence of oxygen vacancies introduced during the synthesis of the nanomaterial. Typically, the presence of these vacancies may in favor of the production of oxidized radical species, the improvement of photocatalytic performance, and the enhancement of light absorption [37,38]. The O 1s XPS spectrum of MoO_3 can be divided into two peaks at 530.6 eV and 531.7 eV, which can be assigned to lattice oxygen in MoO_3 and surface hydroxyl groups, respectively (Fig. 2d) [35]. We note that when the AgI are modified by MoO_3 the peaks of the Mo^{6+} 3d and O^{2-} 1s from MoO_3 in AM-50 display a slight shift toward a high binding energy, which can be attributed to the heterojunction interaction between MoO_3 and AgI. Meanwhile, the Ag 3d core region of AgI shows two peaks at 374.5 and 368.5 eV (Fig. 2e), corresponding to Ag $3d_{3/2}$ and Ag $3d_{5/2}$. And the I 3d XPS spectrum (Fig. 2f) shows two major peaks with binding energies of 631.2 eV and 619.7 eV, which can be ascribed to $3d_{3/2}$ and $3d_{5/2}$ of I^- in AgI [34]. It is obviously that the binding energy of Ag^+ 3d and I^- 3d in AM-50 all display slightly shift to the lower binding energy in comparison with pure AgI, indicating that the chemical coordination environment of Ag^+ and I^- have changed to some extent because of strong interaction between AgI and MoO_3. It is rational to infer that heterojunction have formed between the two materials, which can promote the migration of electron-hole pairs and enhance the photocatalytic performance and stability.

The photocatalytic performance of the as-prepared samples was evaluated by the degradation of SMZ under visible light irradiation. As exhibited in Fig. 3a, SMZ is rarely degraded without the addition of photocatalysts, indicating SMZ is quite stable under visible light irradiation. Meanwhile, pure MoO_3 and AgI exhibit poor photocatalytic activity, whose degradation rate in 20 min are just 10% and 8%, respectively. The photocatalytic degradation efficiency of SMZ is 13.6%, 47.4%, 97.6%, 59.6% and 46.1% for the AM-10, AM-30, AM-50, AM-70, and pm-AM-50 after irradiation for 20 min. Among them, the AM-50 exhibits the highest photocatalytic activity with the rate constant of 0.13 min^{-1} (Fig. S2 in Supporting information). Noted that all the 0D/1D AgI/MoO_3 composites display markedly higher photocatalytic degradation of SMZ than bare MoO_3 and AgI. And the AM-50 nanocomposites exhibit much better photocatalytic activity than that of pm-AM-50, which imply the form of heterostructure interaction between AgI nanoparticles and MoO_3 nanobelts rather than simple physical mixture. The heterostructure brings outstanding photocatalytic performance and promotes the transfer and separation of photogenerated charge carriers, which has already been confirmed by photocurrent curves (PC) and electrochemical impedance spectroscopy (EIS) tests (Fig. S4 in Supporting information). With the increase of AgI load, the photocatalytic performance of 0D/1D AgI/MoO_3 heterostructure composites first increases and then decreases. This probably because that excessive AgI particles have an intense propensity of agglomeration, which restrains their valid contact with MoO_3 nanobelts.

To better reflect the degradation process of SMZ by AgI/MoO_3 composites, the transformation behavior of SMZ during the reaction was investigated by 3D excitation-emission matrix (EEM) spectra (Fig. 3). The general characteristics of the EEM plots for the sample AM-50 show that SMZ has one main peak located at E_x/E_m = 260–300/315–380 nm [39]. Before irradiation, strong extra signals presented in SMZ solution (Fig. 3e). With irradiation time extending, this peak intensity begins to decrease, which attributed to the degradation of SMZ. When the irradiation time increases to 20 min (Fig. 3h), the peak strength of SMZ becomes weak, showing that the SMZ molecules were almost completely degraded by AM-50 composite. The possible degradation pathways of SMZ achieved according to the results of HPLC-MS are shown in Fig. S5 (Supporting information).

To investigate the photocatalytic mechanism, trapping experiments were carried out to quench the main reactive species involved in the degradation of SMZ. The results are shown in Fig. 3b, when using ethylenediaminetetraacetic acid disodium salt (EDTA-2Na) as the direct hole scavenger, a remarkable inhibitory

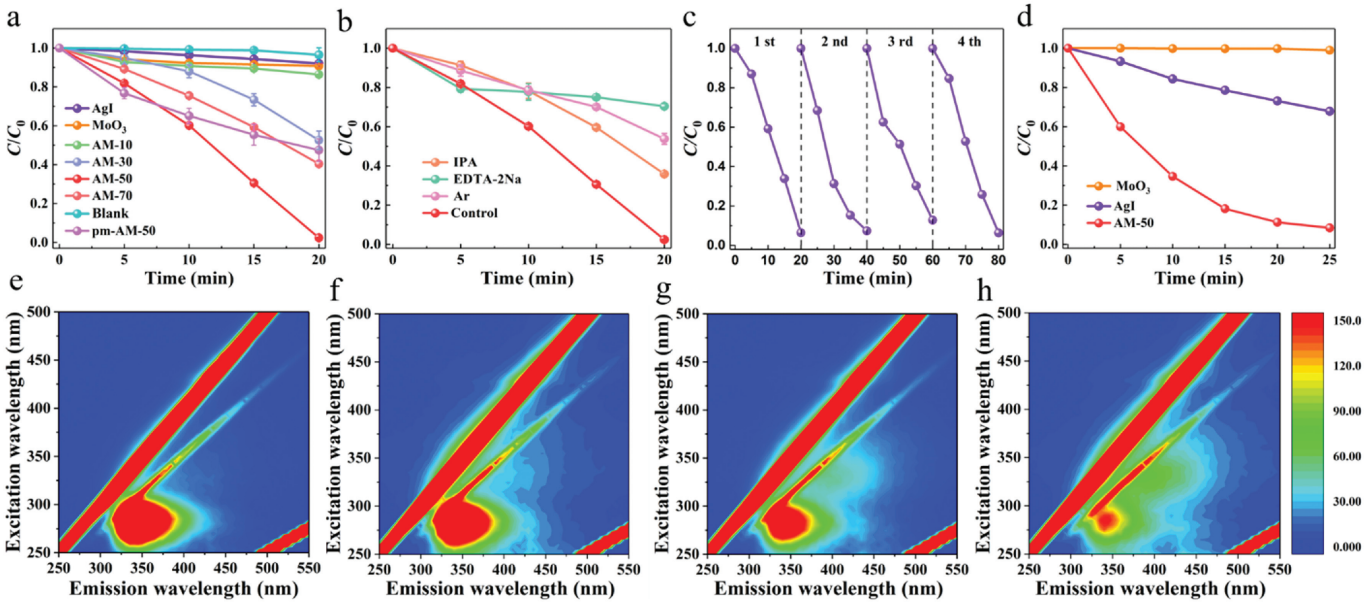

Fig. 3. Photocatalytic degradation of SMZ with AgI/MoO_3 composites (Blank: SMZ degraded under visible light without the addition of photocatalyst) (a); capture experiment of AM-50 for SMZ degradation (b); cycle experiments of AM-50 for SMZ degradation (c); photocatalytic degradation of ACE with AM-50 (d); the 3D EEM spectra of the SMZ solution in AgI/MoO_3 visible system: 0 min (e), 5 min (f), 15 min (g) and 20 min (h).

effect on the degradation efficiency of SMZ is observed and its rate constant *k* value (Fig. S2) is 0.02 min^{-1}, which is far below that of control experiments of AM-50 without scavengers (0.13 min^{-1}). When isopropanol alcohol (IPA) was introduced or Argon was passed through, 64% and 46% of SMZ were degraded. Therefore, hole (h^+), superoxide ($^{\bullet}O_2^-$) and hydroxyl ($^{\bullet}OH$) are all working species in the degradation of SMZ. Among them, h^+ is the leading radical. Moreover, the AM-50 sample maintains effective photocatalytic degradation stability during repeated tests (Fig. 3c). So, it is obvious that AM-50 could work as a high-efficiency photocatalyst for the removal of SMZ in water.

In order to verify the photocatalytic performance of the AM-50, Acetaminophen (ACE) was chosen as another contaminant for degradation under visible-light irradiation. As shown in Fig. 3d, 91.6% of ACE can be removed by AM-50 under visible light for 25 min. While the degradation rate for pure MoO_3 and AgI are 1% and 32%, respectively. The results indicate that the AM-50 heterostructures do have outstanding photocatalytic degradation capability.

The electron spin resonance (ESR) technology was used to detected short-lived active species in the degradation process. As shown in the diagram Fig. 4, typical peaks of $^{\bullet}O_2^-$ were clearly recorded in DMPO-$^{\bullet}O_2^-$ spectra after 10 min visible light irradiation, while there is no obvious signal appeared in the dark. As for $^{\bullet}OH$, compared with the dark condition, four evident peaks of 1:2:2:1 proportion appeared under irradiation, which is powerful evidence of the generation of $^{\bullet}OH$. The above results demonstrate convincingly that $^{\bullet}O_2^-$ and $^{\bullet}OH$ are produced and participated in the photocatalytic degradation process of SMZ.

In the light of the active species verification test and the band position of each photocatalytic material obtained from the diffuse reflectance spectra (DRS) (Fig. S3 in Supporting information) and empirical equation, the possible carriers transfer path and photocatalytic mechanism of 0D/1D AgI/MoO_3 heterostructures is proposed. Under the irradiation of visible light, the photogenerated electrons would be inspired and then transfer form VB to CB both in MoO_3 and AgI. If the carriers transfer following a traditional type-II heterojunction (Fig. S6 in Supporting information), the electrons on the CB of AgI would shift to the CB of MoO_3 and the holes on the VB of MoO_3 would move to the VB of AgI, leaving electrons on the CB (0.35 V) of MoO_3 and holes on the VB (2.39 V) of AgI which cannot satisfy the reduction potential of $O_2/^{\bullet}O_2^-$ (–0.33 V *vs.* NHE) [40] and the oxidation potential of $H_2O/^{\bullet}OH$ (2.68 V *vs.* NHE) [32]. Hence, a Z-system heterojunction may be a reasonable way to explain the photocatalytic reaction mechanism. As is illustrated in Fig. 4c, after being inspired by visible light, the electrons accumulated on the CB of MoO_3 would transfer and recombine with the holes on the VB of AgI. Thus, the photogenerated electrons at the CB of AgI (–0.43 V) and the holes at the VB of MoO_3 (3.44 V) could be retained, which ensures a strong redox capability for the generation of reactive species, such as $^{\bullet}O_2^-$ and $^{\bullet}OH$, that are highly efficient for the degradation of SMZ. The assumption is consistent with the results of the above tests.

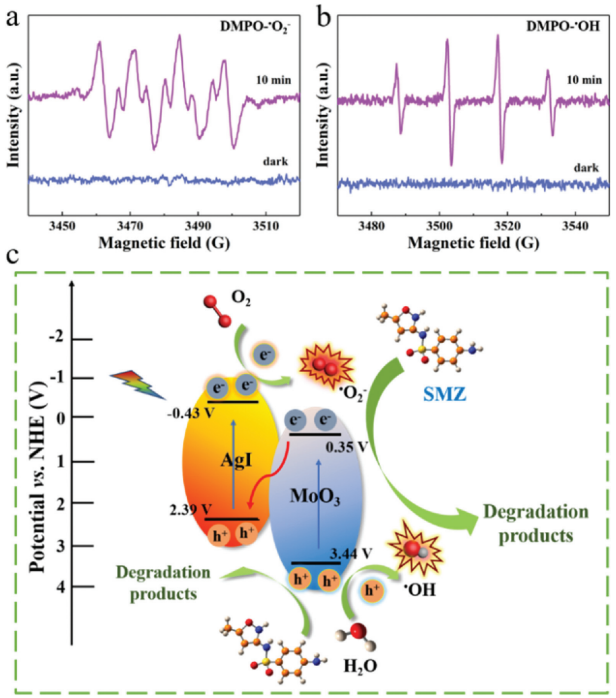

Fig. 4. ESR spectra of the DMPO-$^{\bullet}O_2^-$ (a), and DMPO-$^{\bullet}OH$ (b) adducts recorded with pristine AM-50 in the dark and under visible light irradiation. Scheme diagram of possible photocatalytic mechanism of AM-50 (c).

Overall, a novel 0D/1D AgI/MoO_3 Z-system heterostructure was successfully synthesized. The optimum composite sample AM-50 presented outstanding photocatalytic performance for both SMZ and ACE degradation. Compared with single MoO_3 and AgI, the degradation efficiency of SMZ by AM-50 increased by 87% and 89%, respectively. Meanwhile, the increasement of ACE degradation efficiency depended on AM-50 was up to 90% and 59%, when compared with MoO_3 and AgI, respectively. The 0D/1D nano heterostructure plays the key role in the increased exposure of active sites and the accelerated separation of photogenerated charge carriers, which brings excellent photocatalytic properties and stability. It is the first time that the MoO_3-based photocatalytic samples have been used in SMZ degradation, which is a worthwhile attempt that widen the road of MoO_3-based photocatalysts in PPCPs degradation. Based on this study, the construction of other low dimension MoO_3-based heterostructure system materials could be considered.

Declaration of competing interest

The authors report no declarations of interest.

Acknowledgments

This work was financially supported by the National Key Plan for Research and Development of China (No. 2016YFC0502203), Natural Science Foundation of China (No. 51979081), Fundamental Research Funds for the Central Universities (No. B200202103), National Science Funds for Creative Research Groups of China (No. 51421006), the Key Program of National Natural Science Foundation of China (No. 91647206), and the Priority Academic Program Development of Jiangsu Higher Education Institutions (PAPD).

Appendix A. Supplementary data

Supplementary material related to this article can be found, in the online version, at doi:https://doi.org/10.1016/j.cclet.2021.04.003.

References

[1] Y. Yang, Y.S. Ok, K.H. Kim, et al., Sci. Total Environ. 596 (2017) 303–320.
[2] X. Feng, P. Wang, J. Hou, et al., Chem. Eng. J. 352 (2019) 947–956.
[3] H. Hai, X. Xing, S. Li, et al., Sci. Total Environ. 738 (2020) 265–283.
[4] D. Song, W.A. Jefferson, H. Cheng, et al., Chemosphere 222 (2019) 71–82.
[5] S. He, C. Zhai, M. Fujitsuka, et al., Appl. Catal. B: Environ. 281 (2021) 119479.
[6] M. Zhu, L. Zhang, S. Liu, et al., Chin. Chem. Lett. 31 (2020) 1961–1965.
[7] Y. Ao, L. Xu, P. Wang, et al., Dalton Trans. 44 (2015) 11321–11330.
[8] S. Zhou, Y. Wang, K. Zhou, et al., Chin. Chem. Lett. 32 (2021) 2179-2182..
[9] X. Hu, X. Hu, Q. Peng, et al., Chem. Eng. J. 380 (2020) 122366.
[10] E. Adamek, W. Baran, A. Sobczak, Process Saf. Environ. Prot. 103 (2016) 1–9.

[11] M. Tang, Y. Ao, P. Wang, et al., J. Hazard. Mater. 387 (2020) 121713.
[12] Z. Xie, Y. Feng, F. Wang, et al., Appl. Catal. B: Environ. 229 (2018) 96–104.
[13] D. Wang, Y. Ao, P. Wang, Sci. Total Environ. 746 (2020) 141149.
[14] Y. Zhang, S.J. Park, J. Catal. 361 (2018) 238–247.
[15] Y. Zhang, S.J. Park, J. Mater. Chem. A: Mater. Energy Sustain. 6 (2018) 20304–20312.
[16] W. Yang, J. Xiao, Y. Ma, et al., Adv. Energy Mater. 9 (2019) 1803137.
[17] S.L. Prabavathi, P.S. Kumar, K. Saravanakumar, et al., J. Photochem. Photobiol. A: Chem. 356 (2018) 642–651.
[18] Y. Zhang, S.J. Park, Appl. Catal. B: Environ. 240 (2019) 92–101.
[19] C. Lai, M. Zhang, B. Li, et al., Chem. Eng. J. 358 (2019) 891–902.
[20] J. Hu, D. Chen, Z. Mo, et al., Angew. Chem. Int. Ed. 58 (2019) 2073–2077.
[21] H. Zhang, J. He, C. Zhai, et al., Chin. Chem. Lett. 30 (2019) 2338–2342.
[22] Y.B. Chen, J.F. Li, P.Y. Liao, et al., Chin. Chem. Lett. 31 (2020) 1516–1519.
[23] K.Z. Li, C.Y. Zhang, X. Li, et al., Catal. Today 335 (2019) 173–179.
[24] M. Ren, Y. Ao, P. Wang, et al., Chem. Eng. J. 378 (2019) 122122.
[25] S. He, C. Yan, X.Z. Chen, et al., Appl. Catal. B: Environ. 2 (2020) 119138.
[26] P. Zhou, J. Yu, M. Jaroniec, Adv. Mater. 26 (2014) 4920–4935.
[27] W. Zhang, A.R. Mohamed, W.J. Ong, Angew. Chem. Int. Ed. 59 (2020) 22894–22915.
[28] K. Maeda, ACS Catal. 3 (2013) 1486–1503.
[29] X.J. Wen, C.H. Shen, Z.H. Fei, et al., Chem. Eng. J. 383 (2020) 123083.
[30] Y. Yang, Z. Zeng, C. Zhang, et al., Chem. Eng. J. 349 (2018) 808–821.
[31] T. Wang, W. Quan, D. Jiang, et al., Chem. Eng. J. 300 (2016) 280–290.
[32] M. Tang, Y. Ao, C. Wang, et al., Appl. Catal. B: Environ. 270 (2020) 118918.
[33] M. Tang, Y. Ao, C. Wang, et al., Appl. Catal. B: Environ. 268 (2020) 118395.
[34] X.J. Wen, L. Qian, X.X. Lv, et al., J. Hazard. Mater. 385 (2020) 121508.
[35] W. Teng, X. Tan, X. Li, et al., Appl. Surf. Sci. 409 (2017) 250–260.
[36] M.T. Qamar, M. Aslam, Z.A. Rehan, et al., Chem. Eng. J. 330 (2017) 322–336.
[37] J. Peña-Bahamonde, C. Wu, S.K. Fanourakis, et al., J. Catal. 381 (2020) 508–519.
[38] Y. Wu, H. Wang, W. Tu, et al., Appl. Organomet. Chem. 33 (2019) e4780.
[39] S. Li, F. Wang, W. Pan, et al., Chem. Eng. J. 373 (2019) 995–1002.
[40] Z. Wu, Y. Liang, X. Yuan, et al., Chem. Eng. J. 394 (2020) 124921.